Journal of Optics

PAPER

Towards attosecond-scale highly directed GeV gamma-ray sources with multipetawatt-class lasers

To cite this article: A V Bashinov *et al* 2017 *J. Opt.* **19** 114012

View the article online for updates and enhancements.

Related content

- Quantum radiation reaction in head-on laser-electron beam interaction
  Marija Vranic, Thomas Grismayer, Ricardo A Fonseca et al.
- Quantum-electrodynamic cascades in intense laser fields
  N B Narozhny and A M Fedotov
- Strong field interaction of laser radiation
  Alexander Pukhov

This content was downloaded from IP address 195.122.226.14 on 20/12/2017 at 15:42

IOP Publishing Journal of Optics
J. Opt. **20** (2018) 019502 (2pp) https://doi.org/10.1088/2040-8986/aa9f4e

Corrigendum: Towards attosecond-scale highly directed GeV gamma-ray sources with multipetawatt-class lasers (2017 *J. Opt.* 19 114012)

A V Bashinov[1], E S Efimenko[1], A A Gonoskov[1,2,3], A V Korzhimanov[1,3], A A Muraviev[1], A V Kim[1] and A M Sergeev[1]

[1] Institute of Applied Physics RAS, Ulyanov Street, Nizhny Novgorod 603950, Russia
[2] Department of Physics, Chalmers University of Technology, SE-41296 Gothenburg, Sweden
[3] Lobachevsky State University of Nizhni Novgorod, Nizhny Novgorod 603950, Russia

E-mail: bashinov@appl.sci-nnov.ru

Received 23 November 2017
Accepted for publication 5 December 2017
Published 20 December 2017

(Some figures may appear in colour only in the online journal)

The authors apologize that figure 7 was incorrect due to technical errors made while operating with data of numerical simulations. The script processing data had programming errors and confusion of parameters for the test and final simulations.

First, there was an excessive time shift between the laser pulse (blue dashed line) and the pulse of GeV photons (red solid line) in figures 7(a)–(c), coming from test simulations where boundary spheres had a larger radius. Second, inappropriate division of integer by integer resulted in an incorrect normalization of the vacuum field envelope (blue dotted line) and electric field oscillations (blue dashed line). In figures 7(b) and (c), the envelope did not reach unity and electric field oscillations were excessively large in comparison with the envelope in figures 7(a)–(c). Third, in figure 7(c) an isolated attosecond gamma-ray burst of photons with energy greater than 3 GeV was replaced, by mistake, by the two-peak femtosecond pulse corresponding to photons with energy greater than 2 GeV. This led to the contradiction with the conclusion about the generation of an isolated attosecond gamma ray pulse on page 9. Figure 8 confirms this incorrect substitution. This figure shows that gamma-ray pulses corresponding to photons with energy less than 2.2 GeV have femtosecond duration, while isolated attosecond pulses are generated at a higher photon energy range.

The authors emphasize that these errors compromised only the presentation of the results concerning the generation of attosecond pulses, but not the results themselves. The corrected figure 7 is shown below. The revised figure does not affect any other results or conclusions of the article.

 © 2017 IOP Publishing Ltd Printed in the UK

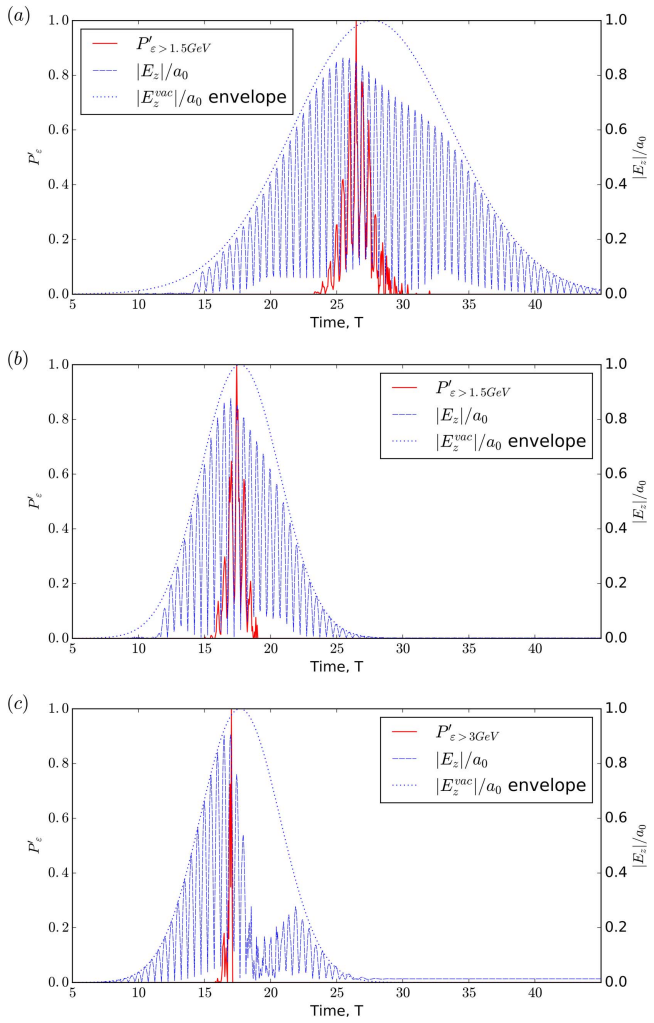

Figure 7. Time distribution of generated gamma radiation for (a) 30 fs, (b) 15 fs laser pulses with peak power 15 PW and (c) 15 fs laser pulse with peak power 40 PW. Spectral power of gamma radiation (red solid line) corresponds to photons with energy higher than (a), (b) 1.5 GeV and (c) 3 GeV. Blue dashed line describes oscillations of electric field in focus, blue dotted line shows vacuum pulse envelope.

ORCID iDs

A V Bashinov https://orcid.org/0000-0001-5838-2249

IOP Publishing Journal of Optics
J. Opt. 19 (2017) 114012 (9pp) https://doi.org/10.1088/2040-8986/aa90a7

Towards attosecond-scale highly directed GeV gamma-ray sources with multipetawatt-class lasers

A V Bashinov[1], E S Efimenko[1], A A Gonoskov[1,2,3], A V Korzhimanov[1,3], A A Muraviev[1], A V Kim[1] and A M Sergeev[1]

[1] Institute of Applied Physics RAS, Ulyanov Street, Nizhny Novgorod 603950, Russia
[2] Department of Physics, Chalmers University of Technology, SE-41296 Gothenburg, Sweden
[3] Lobachevsky State University of Nizhni Novgorod, Nizhny Novgorod 603950, Russia

E-mail: bashinov@appl.sci-nnov.ru

Received 30 June 2017, revised 23 September 2017
Accepted for publication 3 October 2017
Published 25 October 2017

Abstract

We consider a possibility of constructing a gamma-ray source based on the multibeam configuration of a multipetawatt laser system which we simulate using a converging dipole wave. It is shown that such a configuration of fields allows the generation of gamma radiation with narrow directivity of about 1 mrad in the form of pulse trains or isolated pulses on the attosecond timescale. The influence of quantum electrodynamic cascade development on the parameters of generated gamma bursts is studied.

Keywords: gamma radiation, QED cascade, multipetawatt lasers

(Some figures may appear in colour only in the online journal)

1. Introduction

Recent advances in laser technology have allowed the development of petawatt-class laser facilities capable of providing an intensity of more than 10^{22} Wcm^{-2} [1]. Experiments using the latest generation of high-power laser systems have led to the observations of many breakthrough effects, including the advanced achievements such as laser-based generation of ultrarelativistic electron beams [2] and energetic protons [3, 4]. Moreover, these systems allow creating beams of high-energy photons with high brightness and short pulse duration, e.g. coherent pulses by high-order harmonic generation [5] and gamma rays by Compton scattering [6, 7]. Bright achievements are also laser induced nuclear reactions [8, 9] and generation of huge magnetic fields as a result of laser-plasma interaction [10]. The next generation of multipetawatt-class lasers such as ELI [11], Apollon 10 [12], Vulcan10 [13], XCELS [14], and other projects have stimulated further fundamental and applied studies into the interaction of extremely intense laser fields with matter [15]. It was found that the remarkable feature of these interactions is the decisive role of the hard photon emission by charged particles and the efficient conversion of laser energy into gamma rays during the laser-plasma interactions [16–22]. Gamma radiation has important applications in various fields of human activities: in medicine, materials science, and nuclear physics. Moreover, the gamma radiation opens up an opportunity to understand deep processes taking place in the Universe, for example, by analyzing signals coming from compact objects such as pulsars, quasars, and black holes. New projects such as ELI-NP [23], MEGaRay [24], and HIγS [25] can contribute significantly to the various fields of activity ranging from the production of special radioisotopes to the radioactive waste management [9]. These projects aimed at a high spectral density of the gamma radiation open up unique perspectives for a new stage of photonuclear science.

This work is devoted to the possibility of developing gamma-ray sources in the GeV energy range based on laser-plasma interaction when QED cascades are considerable [26–32]. In the framework of the recent concept [30] proposing to use multipetawatt colliding laser beams tightly focused in the form of a dipole wave, we show that generated gamma radiation can have ultrashort duration and narrow directivity. In such extreme fields, the electron motion changes drastically due to the impact of photon emission and the

 © 2017 IOP Publishing Ltd Printed in the UK

corresponding radiation reaction effects [33–42]. As a consequence, a new type of particle motion trajectories can be formed which is referred to as the anomalous radiative trapping (ART) attractor [36, 42]. The peculiarity of this attractor is that particles move within high field regions, thereby additionally intensifying gamma-ray emission. Electrons moving along the attractor can lose a substantial part of their energy in an act of GeV photon emission, and high energy photons are generated in the form of short flashes that propagate predominantly along the electric field. However, at such high intensities the abundant electron–positron pair creation coupled with gamma-ray emission and gamma photon decay emerges [43]. On the one hand, the cascade can intensify gamma radiation, pulling the electron–positron plasma into the electric field antinode region [28]. But, on the other hand, it can strongly modify the radiation spectrum due to different spectral probability densities of photon emission and decay. These capabilities of the cascade must be studied in order to understand the possibility of creating a laser-plasma-based source of gamma radiation. Since the QED effects are very sensitive to field strength [26, 44], we consider the field configuration in the form of a dipole wave [45] providing an utmost field localization and maximizing the field strength in focus for a given laser power. Such a field configuration can be well mimicked by a multi-beam configuration of a laser system, for example, the XCELS project proposes focusing of 12 multipetawatt beams [14]. Another advantage of extreme focusing for a gamma-ray source is that the generated photons can quickly leave the interaction region without decaying into electron–positron pairs. We pay particular attention not only to the energy spectrum and the time distribution of the generated gamma rays, but also to the features of the radiation pattern stipulated by the cylindrical symmetry of the field configuration.

2. QED cascade and electron–positron plasma distribution

The properties of radiation generated by a particle during curvilinear motion in a laser field depend on particle momentum and its direction relative to electric and magnetic fields, as well as on field values themselves [46]. In the case of tight focusing, these factors acquire additional significance, since the scale of the particle oscillations becomes comparable with the scale of the field inhomogeneity. To understand the spectral properties of plasma radiation, it is necessary to ascertain its distribution in a laser field. Note that despite stochastic photon emission in the ART regime, the plasma motion is more or less synchronized and its dynamics can be described by the motion of a single particle. In this regime, it should also be taken into account that the amplitude of electric field and field structure in the vicinity of the electric field antinode strongly influence plasma distribution. However, the development of the QED cascade even in a given field can greatly change the distribution function of a particle in spatial and momentum spaces. In the present paper, we confine ourselves to analysis of the linear stage of the cascade, when back reaction of the created plasma can be neglected and the laser field is assumed to have vacuum distribution. To intensify QED effects, we consider a tightly focused field in the form of a dipole wave [45] shown in figures 1(a)–(d). The structure of the wave is symmetric with respect to the z axis along which the electric field is directed. The magnetic field has a toroidal structure. For detailed analysis of plasma-field distributions and the spectra of plasma radiation in these fields, we used the PIC-code PICADOR [47]. For simulation of QED cascades, we consider a plasma seed target with density $n_e = 10^{15}$ cm^{-3} initially having the form of a cylinder with altitude λ_L along the z axis and radius of $0.5\lambda_L$, where λ_L is the wavelength of a dipole wave. For analysis, we used a half infinite dipole wave with one laser cycle leading edge and the wavelength $\lambda_L = 0.9\ \mu$m. The simulation box had the size $4\ \mu\text{m} \times 4\ \mu\text{m} \times 4\ \mu$m and included $512 \times 512 \times 512$ cells. The time step was $0.03\omega_L^{-1}$, where ω_L is the laser frequency. To take into account QED processes within the frame of the local constant field approximation [48–50], we used a QED adaptive event generator [51] which allows switching on/off photon decays. Simulation results of QED cascades in the fields of dipole waves with different powers are shown in figures 1(e)–(l). Because of the field symmetry, the generated plasma is uniform along the azimuth angle (measured in a plane perpendicular to the z axis). In a dipole wave, because of the field inhomogeneity, the particles can not only be trapped in the ART regime, but can also leave the strong field region. Generally, particles accelerated by an electric field escape along the z axis, without losing their energy on radiation, because the magnetic field in this region is weak and cannot turn them back into the interaction region. Since particle escape slows down due to trapping and the pair creation growth rate increases with increasing wave power, there is a threshold of cascade development $P_{\text{th}} \equiv 7.2$ PW [30] when the particle escape is balanced by pair creation.

For qualitative analysis, it is convenient to distinguish two different cases. The first one is when the laser power slightly exceeds the cascade development threshold, namely $0 < P - P_{\text{th}} \ll P_{\text{th}}$. In this case, the cascade growth rate Γ is much smaller than the laser frequency ω_L and the particles have enough time to approach the attractor. Plasma distributions with (figures 1(e) and (f)) and without (figures 1(g) and (h)) cascade taken into account are similar: plasma distributed in the form of letter 'C' corresponds to the ART regime and there are also particles forming a thin ring at the electric field node in the regime of normal radiative trapping (NRT) [35, 36]. In the latter regime, particles have much less energy and their contribution to the radiation spectrum can be neglected. Nevertheless, one can distinguish the difference in plasma distribution due to cascade development. There are more particles close to the z axis, and plasma density has a local maximum at the point of maximum electric field amplitude (coordinate origin in figure 1(e)), while without cascade it has a local minimum at this point (figure 1(g)).

In the second case of appreciable excess of the threshold, $\Gamma > \omega_L$ and the development of the cascade itself mainly determines the structure of the plasma, since the characteristic

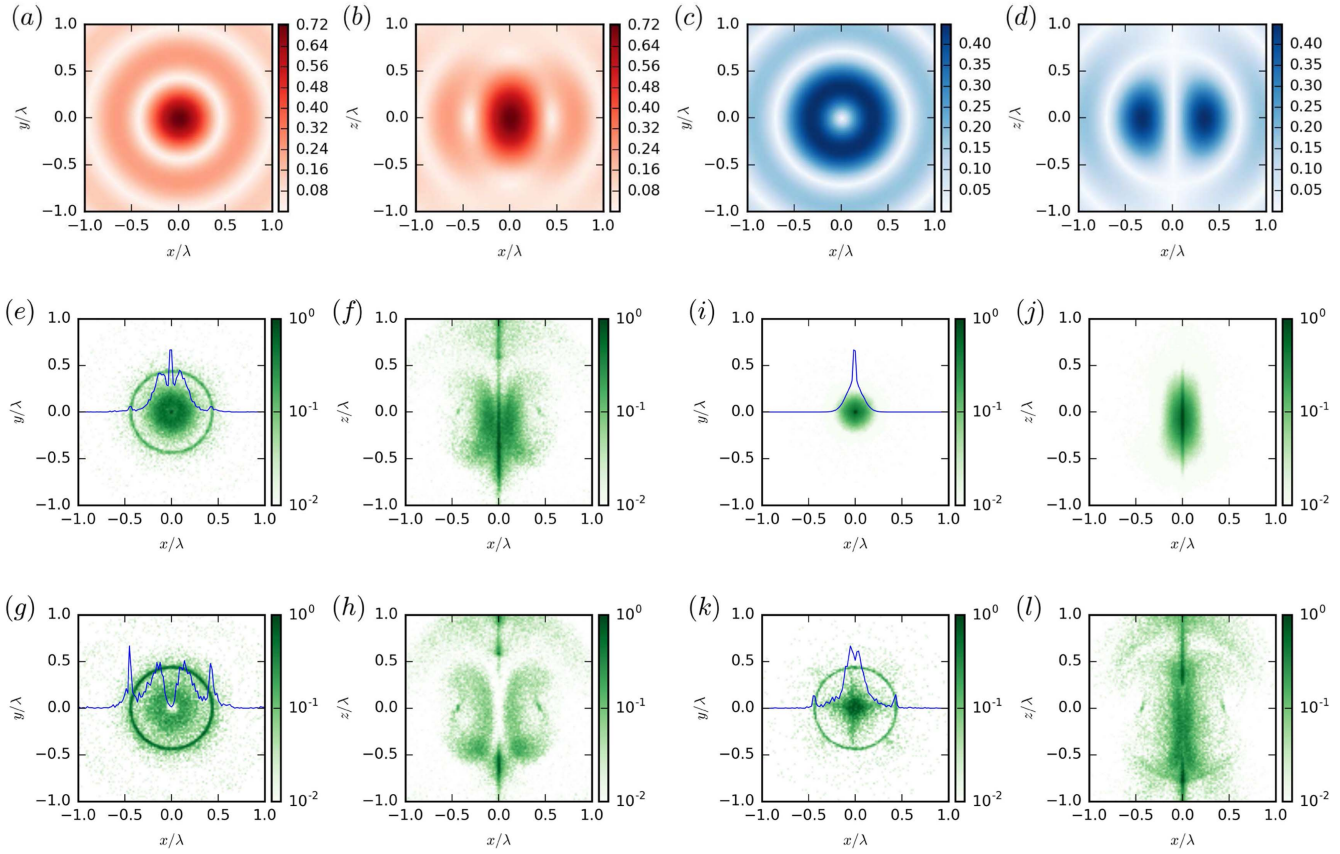

Figure 1. Spatial distribution of (a), (b) electric and (c), (d) magnetic fields of dipole wave in planes xy (a), (c) and xz (b), (d). Electron distribution due to cascade development in dipole wave is depicted in planes xy (e), (i) and xz (f), (j). Similar distributions obtained without pair creation are shown in (g), (k) and (h), (l), respectively. (e)–(h) Correspond to $P = 10$ PW, while (i)–(l) correspond to $P = 100$ PW. Blue solid lines in figures (e), (i), (g) and (k) show normalized plasma profile plotted on a linear scale along the line $y = 0$.

time of pair creation is much shorter than the characteristic time of particle motion (figures 1(i) and (j)). Plasma density has a maximum along the z axis and the distribution profile of particles in the ART regime is hardly distinguishable. The ring of NRT particles is completely invisible. On the contrary, without pair creation (figures 1(k) and (l)) plasma density has local minimum at the point of the coordinate origin. The blue line in figure 1(k) and the light green region along $x = 0$ in figure 1(l) demonstrate this minimum. There is also an evident pattern of NRT particles. It is important to note that for higher wave powers ART particles are closer to the z axis (compare figures 1(g) and (k)). Computer simulations show that on the average particles are at the distance $\rho_{\mathrm{ART}} \approx 0.27P^{-0.2}\lambda_L$ from the axis, where P is given in PW.

Summarizing the simulation results, we can conclude that the QED cascades lead to redistribution of electron–positron plasma providing evident presence of pair plasma at the electric field antinode. In case of small excess of the threshold power, the change of plasma distribution due to the cascade is not crucial. Plasma dynamics in ART and NRT regimes forms typical patterns, but in addition there appears the maximum of plasma density at the point of the electric field antinode. Note that ART particles are at the distance ρ_{ART} from the antinode, on the average, and are not a cause of this maximum. However, in case of substantial excess of the threshold power, the cascade mainly determines the plasma structure which becomes strongly peaked at the antinode. ART and especially NRT plasma patterns are evanescent in comparison with this peak.

3. Energy spectrum

In this section, we consider the radiation spectrum of ART particles and identify the changes introduced by a QED cascade. In general, ART and newly created particles behave in a similar manner. They move in the vicinity of electric field antinode approximately along the field while the electric field amplitude exceeds the magnetic field amplitude, and after that they escape from the interaction region or become trapped for the next half-period. However, there are two important distinctions between these types of particles related to the lifetime in the focal region and the proximity of the particles to the symmetry axis z. ART particles remain in the trapped state longer, while new particles created at random moments of time, in random positions, with random momenta have more probability to escape. At the same time a considerable part of newly created particles are closer to the z axis, and they can emit photons with higher energy. To get a qualitative understanding of the spectrum of gamma radiation, we pay attention to the time interval when the ART particles

accelerated in the electric field begin to rotate in the magnetic field (turning phase), emitting a considerable part of their energy. The importance of this interval is also stipulated by the fact that the radiation emitted along the electric field can be rapidly released, while photons propagating in other directions have a longer path in a strong field and, consequently, a higher probability to decay. A particle accelerated by the electric field can gain a maximum Lorentz factor $\gamma_e^{\max} \sim a$ [36], where a is the amplitude of the electric field in focus normalized to the relativistic field and is related to the laser power as [45]

$$a \approx 800\sqrt{P[\mathrm{PW}]}. \tag{1}$$

Below, we omit the power unit PW. Numerical simulations give a more accurate estimate of the maximum Lorentz-factor $\gamma_e^{\max} \approx 1200\sqrt{P} \approx 1.5a$. However, due to the stochasticity of photon emission, the electron energy is a random variable. Averaged over many realizations of particle trajectory or particle ensemble, maximum energy is $\gamma_e^{\mathrm{av}} \approx 400\sqrt{P} \approx 0.5a$. Along with the particle energy there is an important quantum parameter determining the radiation spectrum [52, 53]

$$\chi = \frac{e\hbar}{m^3c^4}\sqrt{(\varepsilon\mathbf{E}/c + \mathbf{p}\times\mathbf{B})^2 - (\mathbf{p}\cdot\mathbf{E})^2}, \tag{2}$$

where $\hbar$ is the Planck constant; m and e are the electron mass and charge; c is the light velocity; ε and p are the energy and the momentum of a particle (electron, positron, photon); E and B are electric and magnetic fields. By analogy with the electron energy, the maximum value of electron quantum parameter is $\chi_e^{\max} \approx P$ [30], and the ensemble averaged value is $\chi_e^{\mathrm{av}} \approx 0.7P^{0.8}$. The difference in the power law of these values is caused by the dependence of the average particle distance from the z axis on P: $\chi_e^{\mathrm{av}} \propto \gamma_e^{\mathrm{av}}\rho_{\mathrm{ART}}B_0 \propto P^{0.8}$, where B_0 is the maximum magnetic field amplitude. In the ultrarelativistic case after photon emission, a particle retains a $1-\delta$ part of the initial values of energy γ_e and quantum parameter χ_e, while a photon receives $\varepsilon_\gamma = \delta\gamma_e$, $\chi_\gamma = \delta\chi_e$, where the photon energy is normalized to the electron rest energy and $\delta \in [0.1]$. In this case, the spectral probability density of photon radiation W'_δ as a function of δ [54] normalized to the inverse wave period $T = 2\pi/\omega_L$ is

$$W'_\delta(P,\delta) = \frac{2\alpha}{\sqrt{3}\,\eta\gamma_e}\left(\int_{y_0}^{\infty} K_{5/3}(y)\mathrm{d}y + \frac{\delta^2}{(1-\delta)}K_{2/3}(y_0)\right), \tag{3}$$

where α is the fine structure constant; $y_0 = 2\delta/[3\chi_e(1-\delta)]$; $\eta = \hbar\omega_L/(mc^2)$. First, from this function follows that the maximum photon energy corresponds to $\delta \approx 1$ (see also figure 2) in quantum regime ($\chi_e > 1$), thus maximum expected photon energy is $\varepsilon_\gamma^{\max} \approx \gamma_e^{\max} \approx 1200\sqrt{P}$. Second, W'_δ has a singularity at $\delta = 0$, and diverges as $W'_\delta \propto \delta^{-2/3}$, this means that a particle emits many photons with low energies. Third, the average photon energy can be estimated as

$$\varepsilon_\gamma^{\mathrm{av}}(P) = \gamma_e^{\mathrm{av}}\int W'_\delta(P,\delta)\,\delta\,\mathrm{d}\delta\left(\int W'_\delta(P,\delta)\mathrm{d}\delta\right)^{-1}. \tag{4}$$

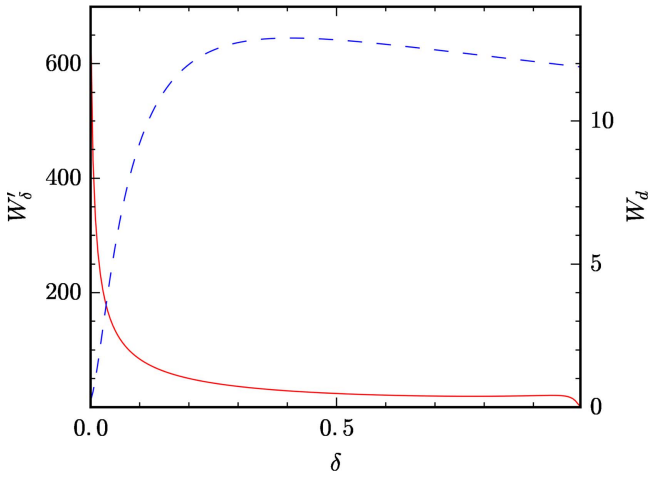

Figure 2. Probability of photon emission W'_δ (solid line) and photon decay W_d (dashed line) as a function of δ for $P = 100$ PW.

If $P \to \infty$ and consequently $\chi_e \to \infty$, the limit of this value is $\varepsilon_\gamma^{\mathrm{av}}(P) \approx 0.25\gamma_e^{\mathrm{av}}(P)$. Thus, in the ART regime at $P \gg P_{\mathrm{th}}$ the electron quantum parameter is $\chi_e \gg 1$ and the average photon energy is $\varepsilon_\gamma^{\mathrm{av}} \approx 100\sqrt{P} \approx \varepsilon_\gamma^{\max}/12$.

However, the photon decay during QED cascades can modify the radiation spectrum. First, pairs created as a result of photon decays lead to spatial redistribution of the plasma (see section 2). Greater parts of the plasma appear at the electric field antinode, which can increase the portion of highly energetic photons. Second, photon decay depends on photon momenta and electromagnetic field, which leads to suppression of different spectral ranges. For determining these ranges, it is necessary to consider the spectral properties of the photon decay. The probability of photon decay [55] normalized to the inverse wave period as a function of photon energy ε_γ and quantum parameter χ_γ has the following form:

$$W_d = \frac{2\alpha}{3\sqrt{3}\,\eta\varepsilon_\gamma}\int_0^1 \frac{9-u^2}{1-u^2}K_{2/3}\left(\frac{8/(3\chi_\gamma)}{(1-u^2)}\right)\mathrm{d}u, \tag{5}$$

and is shown in figure 2. For a given wave power P, the photon quantum parameter is proportional to its energy $\chi_\gamma \propto \varepsilon_\gamma$, thus $W_d \propto \exp[-8/(3\chi_\gamma)]$ is exponentially small at $\chi_\gamma \ll 1$ and decreases at $\chi_\gamma \gg 1$ as $W_d \propto \chi_\gamma^{-1/3}$ [55]. Equation (5) shows that W_d is maximized at the photon quantum parameter $\chi_0 \approx 11$ [55], and W_d is half the maximum value at $\chi_1 \approx 2$ and $\chi_2 \approx 300$.

The obtained estimates of the radiation spectrum and the numerical results are compared in figure 3. In numerical simulations, the radiation spectrum is registered on a sphere with radius $2\lambda_L$ (boundary sphere). This radius is close to the boundary of the computational box, where the fields are much weaker in comparison with the fields in focus, so it is assumed that the photon emission and decay affecting the spectra are negligible at this distance. Without QED cascades, the analytical estimate for maximum photon energy is in a good agreement with the numerical results, but the average energy (4) is overestimated by approximately a factor of 3 (see figure 3(a)). This disagreement is caused by the fact that the estimates are applied to the beginning of the turning phase,

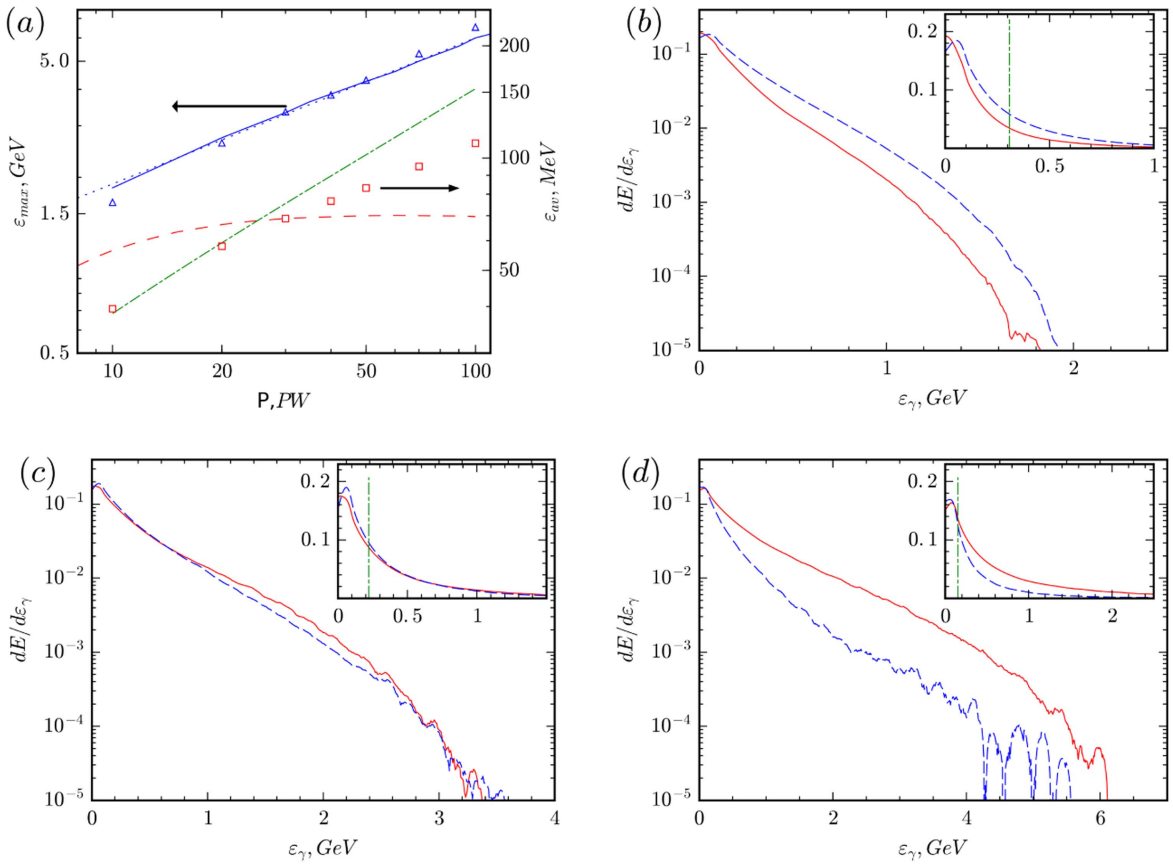

Figure 3. (a) Maximum and average photon energy versus dipole wave power. With the cascade taken into account, maximum and average photon energy are depicted by solid and dashed lines. Curves for maximum and average photon energy obtained without cascade correspond to triangles and squares. Dotted line shows $\varepsilon_\gamma^{\max} \approx 1200\sqrt{P}\,mc^2$. Dashed–dotted line describes estimated average energy according to (4) divided by 3 to fit numerical results. Spectral densities of radiated energy $\mathrm{d}E/\mathrm{d}\varepsilon_\gamma$ obtained with (dashed line) and without (solid line) QED cascade taken into consideration are shown for different powers (b) $P = 10$ PW, (c) $P = 30$ PW, and (d) $P = 100$ PW. The main graphs are on logarithmic scale while the inserts are on linear scale. The vertical dashed–dotted line corresponds to $\delta = 3P^{-0.8}$.

when the most energetic photons are generated, while figure 3(a) shows the radiation spectrum averaged over laser half-period. The spectral densities of radiated photons $\mathrm{d}E/\mathrm{d}\varepsilon_\gamma$ have similar shapes for different powers (see figures 3(b)–(d), solid lines), thus the maximum and average photon energies are proportional to each other, which confirms the estimates. We neglect the influence of particle escape (or particle creation) considering $\mathrm{d}E/\mathrm{d}\varepsilon_\gamma$ normalized to the number of registered photons.

However, QED cascades introduce several properties to the radiation spectrum according to the numerical results shown in figure 3. At $P - P_{\mathrm{th}} \ll P_{\mathrm{th}}$, the maximum value of the photon quantum parameter is $\chi_\gamma^{\max} \sim \chi_e^{\max} \sim 1$ and photons in the $3P^{-0.8} \leqslant \delta \leqslant 1$ range have a higher probability of decay. This range corresponds to $\chi_1 < \chi_\gamma < \chi_e^{\mathrm{av}}$ according to (5) assuming $\chi_\gamma = \delta\chi_e^{\mathrm{av}}$ and $\varepsilon_\gamma = \delta\gamma_e^{\mathrm{av}}$. The cascade is sustained by the most energetic photons at the edge of the spectrum, thus the growth rate is small. At first sight, this leads to suppression of the spectrum edge. On the contrary, numerical simulations show that a cascade enhances generation of high energy photons (figures 3(a) and (b)), because plasma redistribution has a greater influence on the spectrum (see also figures 1(e)–(h)). In this case, both maximum and average photon energy, taking into account QED cascade, are higher than the corresponding values of ART particles.

If $P \gg P_{\mathrm{th}}$, then a significant part of the spectrum $3P^{-0.8} \leqslant \delta \leqslant \min(1; 430P^{-0.8})$ corresponding to photons with quantum parameter $\chi_1 < \chi_\gamma < \min(\chi_e^{\mathrm{av}}; \chi_2)$ is modified. Photons decay rapidly, exerting a greater influence on the spectrum than plasma redistribution. The spectrum in the range specified above is strongly suppressed, which is in agreement with figure 3(d). In this case, the maximum photon energy is slightly decreased in comparison with the ART spectrum, while the average energy is saturated at $\varepsilon_\gamma^{\mathrm{av}} \approx 140$ and even decreases when the power becomes $P > 70$ PW. However, it is important to note that, like in the previous case, QED cascade is mainly sustained by photons with $\delta \sim 3P^{-0.8}$ or $\chi_\gamma \sim 1$, having relatively low energy in this case. This can be explained by comparing the probabilities of photon emission (3) and photon decay (5): at $\delta \ll 1$ the number of photons is proportional to $\delta^{-2/3}$, while the probability of photon decay drops exponentially as $\exp[-8/(3\delta\chi_e^{\mathrm{av}})]$ at $\delta \ll 3P^{-0.8}$ and according to the power law $\delta^{-1/3}$ at $\delta \gg 3P^{-0.8}$.

Thus, a QED cascade has two competitive factors influencing radiation spectrum which clearly manifest themselves in two limiting cases: (i) the power is close to the cascade threshold and (ii) the power is much higher than the cascade threshold. These two qualitatively different cases mean that there is power at which the effect of photon decay is compensated by plasma redistribution. According to the numerical simulations, it occurs at $P \approx 30$ PW (see figure 3(c)).

4. Directivity pattern

Along with the energy spectrum, the angular distribution of radiation is of great importance. Angular distribution is one of the factors determining values of brilliance which can be achieved for utilization. Also, radiation protection strongly depends on the directivity pattern. During laser-plasma interaction it is necessary to understand both angular distribution of radiation of each particle, and how these radiations are combined. The character of particle radiation during QED cascade in the dipole wave inherits the properties of radiation in the ART regime, as the newly created and ART particles have qualitatively similar dynamics. Like in the ART regime, the newly created particles radiate a significant part of their energy at the beginning of the turning phase. During acceleration in the electric field, the particles are located, on the average, at the distance ρ_{ART} and move along the z axis within $-0.25\lambda_L < z < 0.25\lambda_L$. Before the turning phase, particles are, on the average, in the vicinity of the points $z = \pm 0.25\lambda_L$; $\rho = \rho_{\mathrm{ART}}$. By this moment, the magnetic field at particle location reaches maximum strength $B_{\max} = 1.9a\rho_{\mathrm{ART}}\lambda_L^{-1}$ in relativistic units [45]. By rough estimate, the gained maximum transverse momentum is $p_\rho^{\max}/(mc) \approx 0.5B_{\max}\omega_L T/4 \approx 1.5a\rho_{\mathrm{ART}}\lambda_L^{-1}$, as the velocity along the z axis is approximately c and the deviation from the axis lasts $T/4$. Thus, most of the photons are emitted in a cone with half-angle $\Delta\theta = p_\rho^{\max}/(mc\gamma_e) = 1.5a\rho_{\mathrm{ART}}\lambda_L^{-1}\gamma_e^{-1}$ measured from the z axis, where γ_e is Lorentz factor at the beginning of the turning phase. This polar angle $\Delta\theta$ depends on photon energy and wave power. First, an increase of wave power leads to a decrease of $\Delta\theta \propto P^{-0.2}$, because $\gamma_e \propto a$. Second, for highly energetic photons ($\varepsilon_\gamma > \gamma_e^{\mathrm{av}}$) generated by pairs with $\gamma_e \approx \gamma_e^{\max} = 1.5a$ the angular range is $\Delta\theta^{\max} \approx \rho_{\mathrm{ART}}\lambda_L^{-1}$, while for average energy photons ($3P^{-0.8}\gamma_e^{\mathrm{av}} < \varepsilon_\gamma < \gamma_e^{\mathrm{av}}$) generated by pairs with $\gamma_e \approx \gamma_e^{\mathrm{av}} \approx 0.5a$ the angular range is $\Delta\theta^{\mathrm{av}} \approx 3\rho_{\mathrm{ART}}\lambda_L^{-1}$. Low energy photons ($\varepsilon_\gamma < 3P^{-0.8}\gamma_e^{\mathrm{av}}$) have larger angular spread. The dependence of the total energy E'_θ of photons emitted at an angle θ to the z axis during half-period on θ for different photon energy ranges presented in figure 4 agrees with the qualitative estimates. In numerical simulations, the radiation pattern is registered on the boundary sphere with radius $2\lambda_L$. For example, we considered the radiation pattern of the generated plasma in the field of the dipole wave with power $P = 20$ PW. In this case, the highly energetic photons propagate within a cone with angle 0.17 rad, average energy photons with angle 0.3 rad, and low energy photons with angle 0.44 rad. Note that plasma configuration does not influence E'_θ. However, photon energy emitted per solid angle E'_Ω has a distinctive feature related to the cylindrical symmetry of the wave and plasma distribution. It is important that particle motion is plane and can be characterized by azimuth angle φ. During motion each particle emits photons at a certain φ with angular spread $\alpha^* = 1/\gamma_e$. Thus, particles emit most of time in different solid angles and the radiation pattern is wide-angle. However, when the particles' momenta are almost along the z axis, they emit approximately in the same direction, their radiation patterns overlap and are effectively combined. Thus, the major part of energy is emitted along the z axis with angular spread $\sim 1/\gamma_e$ that is in agreement with E'_Ω retrieved from numerical simulations (figure 5). At a large angle $\theta \sim 1$ the properties of $E'_\Omega(\theta)$ are similar to the properties of $E'_\theta(\theta)$. Low energy photons can be emitted at all motion phases, at any solid angle, while high energy photons are more probably emitted only at the beginning of turning phase at $\theta \ll 1$.

It is important to note that, as electrons and positrons move in opposite directions along the z axis, they emit gamma rays in both directions along the axis every half-cycle. In the case of an electron–ion plasma, gamma rays could be emitted alternately along and opposite to the positive direction of the z axis.

5. Time scale of gamma radiation

The time distribution of gamma radiation as well as its directivity pattern depend on the energies of the emitted photons. Low energy photons $\delta < 3P^{-0.8}$ can be emitted at all phases of motion and have a low decay probability. The flux of these photons varies slightly over the period, it is like a gamma ray background. High energy photons are radiated each half-cycle at the beginning of turning phase, so they can form pulses with duration τ as short as a quarter of a period. Moreover, τ can be even shorter than $\pi/(2\omega_L)$ for photons having maximum possible energy for a given wave power. For example, the dependence of gamma-ray bursts duration on photon energy is retrieved from the numerical calculation of the QED cascade in a dipole wave with $P = 20$ PW and is shown in figure 6, where generation of gamma-ray bursts with subfemtosecond duration is confirmed. Although the radiation intensity of the photons with energy $\varepsilon_\gamma < 3P^{-0.8}\gamma_e^{\mathrm{av}} \approx 500$ is weakly modulated over half-period, gamma pulses of high energy photons can be as short as $\pi/(5\omega_L) \approx 300$ as. To describe the generated gamma pulses, we consider the total power P'_ε of gamma radiation in the photon energy range $\varepsilon_\gamma - 0.5\Delta\varepsilon_\gamma < \varepsilon_\gamma < \varepsilon_\gamma + 0.5\Delta\varepsilon_\gamma$ as a function of ε_γ. In computer simulations, the modulation of P'_ε over half-period is registered on the boundary sphere and τ is determined as a full width at the level of $0.5(P'^{\max}_\varepsilon + P'^{\min}_\varepsilon)$, where $P'^{\max,\min}_\varepsilon$ are the maximum and minimum values of the spectral power, respectively. The modulation depth of $P'_\varepsilon(t)$ is characterized by the contrast $r_c = P'^{\min}_\varepsilon/P'^{\max}_\varepsilon$. According to computer simulations, the shape of $\tau(\varepsilon_\gamma)$ becomes almost stabilized if

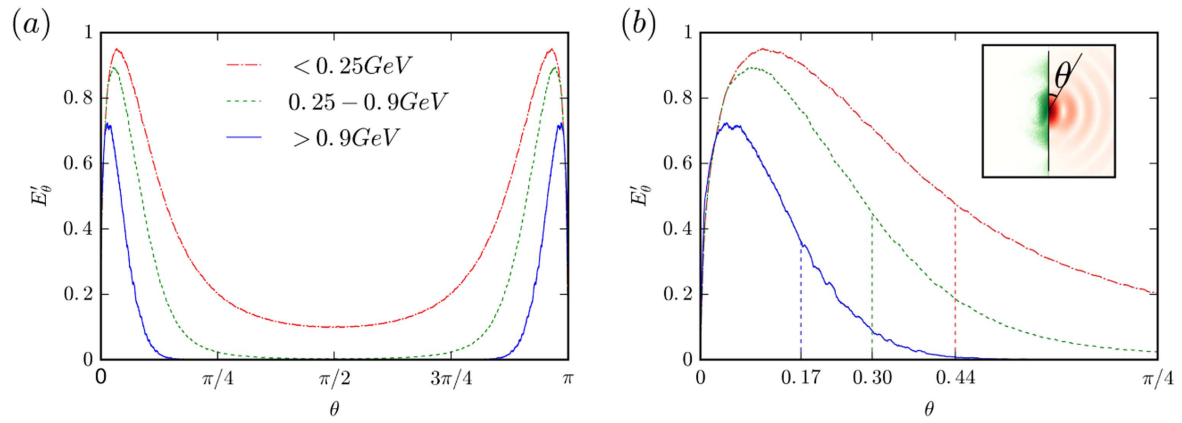

Figure 4. E'_θ as a function of θ for different energy fractions of photons (high, average and low energetic) for 20 PW dipole wave in angular range (a) 0; π and (b) 0; $\pi/4$. Characteristic angle distribution scale is depicted by dashed line for each fraction of particles.

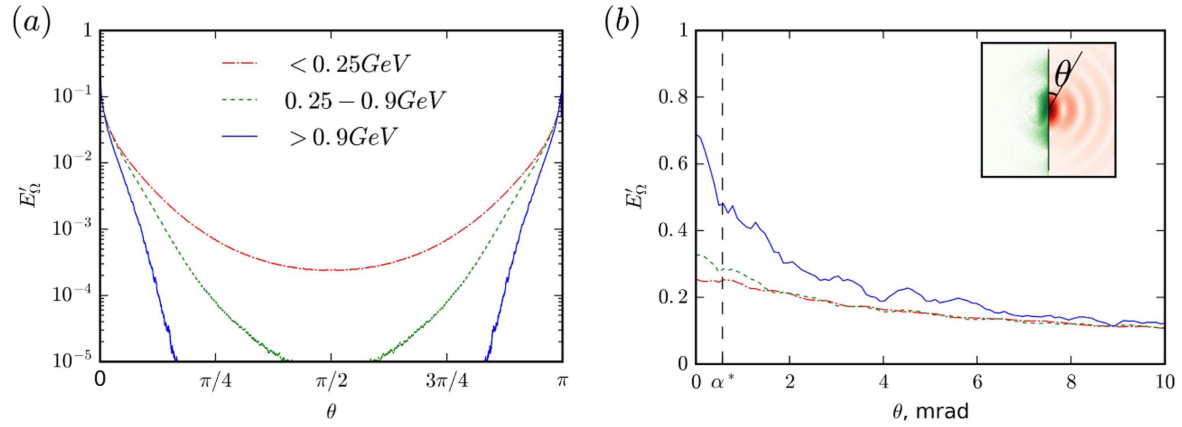

Figure 5. E'_Ω as a function of θ for different energy fractions of photons (high, average and low energetic) for 20 PW dipole wave in angular range (a) 0; π and (b) 0; 10 mrad. Angular spread $\alpha^* = 1/\gamma_e$ is depicted by the black dashed line.

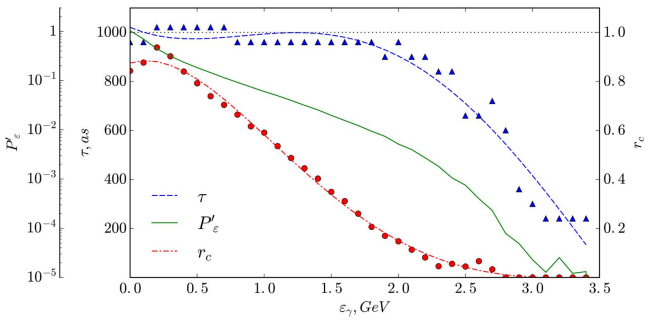

Figure 6. The dependence of gamma ray burst duration, maximum spectral power and contrast on photon energy is reconstructed from numerical calculation of QED cascade in a dipole wave with $P = 20$ PW. Maximum spectral power P'_ε (green line), pulse duration for individual spectral component retrieved from PIC simulation (blue triangles), smoothed approximation of numerical results (blue dashed line), contrast of gamma burst for individual spectral component obtained from PIC simulation (red circles), smoothed approximation of numerical results (red dashed–dotted line). $\Delta\varepsilon_\gamma = 100$ MeV.

$\Delta\varepsilon_\gamma \leqslant 0.05\gamma_e^{\max}$; in figure 6 the energy range $\Delta\varepsilon_\gamma$ is 100 MeV.

Generally, during cascade development, gamma radiation is generated as a train of pulses. The time evolution of spectral power $P'_{\varepsilon>1.5\text{ GeV}}$ for photons with energy greater than 1.5 GeV generated during QED cascade in a dipole wave with peak power $P = 15$ PW and duration $\tau = 30$ fs, initial plasma density being $n_e = 10^{22}$ cm^{-3}, is shown in figure 7(a). Shortening of laser pulse duration decreases the number of gamma ray bursts. If the pulse duration in this example is $\tau = 15$ fs, then the number of gamma ray bursts is approximately halved, figure 7(b). For wave powers close to the threshold P_{th}, the intensity of gamma radiation changes slightly from one half-period to another due to small growth rate Γ, and to produce an isolated attosecond pulse it is necessary to operate with few cycle multipetawatt pulses, filtering a large part of photons and transmitting only the most energetic ones. But for higher wave powers, particle growth is fast $\Gamma > \omega_L$ and the intensity of gamma ray bursts can increase appreciably so that the burst at the next half-period will be much stronger. If the created plasma density reaches an overcritical value, plasma can significantly influence the incident laser pulse, decreasing field intensity and consequently quickly terminating the generation of high energy photons. This allows obtaining an isolated subfemtosecond narrow-directed gamma ray pulse in the GeV energy range. Computer simulations show the feasibility of this approach, for example, for a 15 fs laser pulse with 40 PW peak power

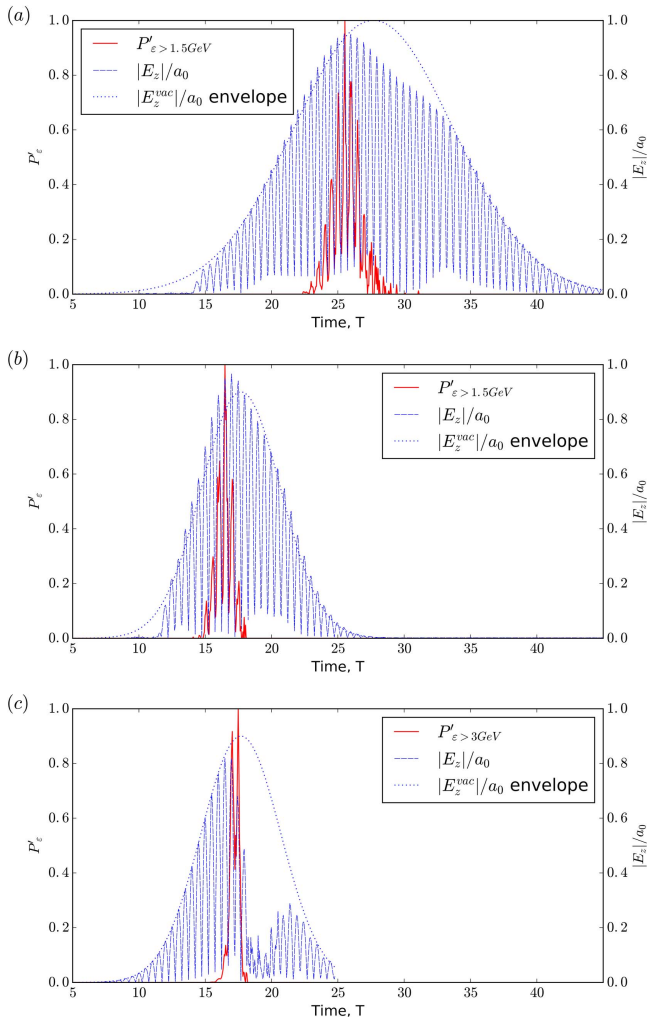

Figure 7. Time distribution of generated gamma radiation for (a) 30, (b) 15 fs laser pulses with peak power 15 PW and (c) 15 fs laser pulse with peak power 40 PW. Spectral power of gamma radiation (red line) corresponds to photons with energy higher than (a), (b) 1.5 GeV and (c) 3 GeV. Blue dashed line describes oscillations of electric field in focus, blue dotted line shows vacuum pulse envelope.

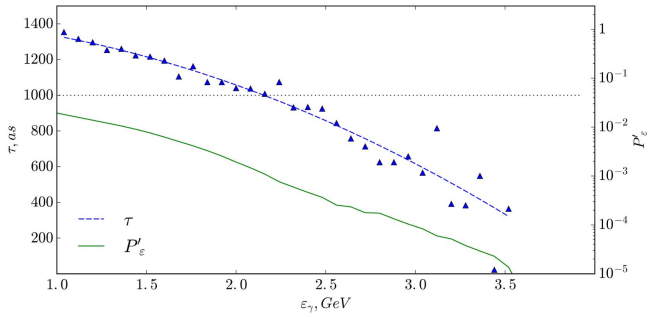

Figure 8. The dependence of gamma-ray bursts duration on photon energy corresponding to 15 fs laser pulse with peak power $P = 40$ PW. Maximum spectral power P'_ε (green line), pulse duration for individual spectral component obtained from PIC simulation (blue triangles), approximation of numerical results (blue dashed line). $\Delta\varepsilon_\gamma = 70$ MeV.

(figure 7(c)), the duration of an isolated gamma-ray pulse is 600 as (FWHM) according to the time evolution of $P'_{\varepsilon>3\,\mathrm{GeV}}$. Moreover, in figure 8, we show that a sub-fs burst as short as 400–500 as can be produced for the most energetic photons in this case $\varepsilon_\gamma > 3.3$ GeV.

6. Conclusion

To conclude, we have considered the properties of gamma radiation generated during the development of a quantum electromagnetic cascade in the field of a converging wave of dipole configuration. Primary attention has been focused on the linear stage of cascade development, that is, the avalanche generation of electron–positron plasma in a given field. Such a study corresponds to the laser pulse durations, when the emerging plasma is not yet capable of influencing the incident field, while the resulting plasma is already a sufficiently effective source of gamma radiation with very unique properties. It is shown that, along with the analysis of the properties of the specific trajectories of individual particles responsible for the generated gamma radiation, it is also necessary to consider the effect of avalanche generation of pairs which essentially determines the particle distribution function over energy states and thus exerts a deterrent influence on the properties of the gamma source. The use of laser pulses of multipetawatt power in the field configuration mimicking a dipole wave makes it possible to generate pulse trains or isolated pulses of gamma radiation in the GeV energy range with duration as short as 300 as with a high radiation directivity.

Acknowledgments

The authors acknowledge the support from the Russian Science Foundation Project No. 16-12-10486.

ORCID iDs

A V Bashinov https://orcid.org/0000-0001-5838-2249

References

[1] Mourou G A, Tajima T and Bulanov S V 2006 *Rev. Mod. Phys.* **78** 309–71
[2] Leemans W P *et al* 2014 *Phys. Rev. Lett.* **113** 245002
[3] Jung D *et al* 2013 *Phys. Plasmas* **20** 083103
[4] Wagner F *et al* 2016 *Phys. Rev. Lett.* **116** 205002
[5] Dromey B *et al* 2006 *Nat. Phys.* **2** 456–9
[6] Corde S, Ta Phuoc K, Lambert G, Fitour R, Malka V, Rousse A, Beck A and Lefebvre E 2013 *Rev. Mod. Phys.* **85** 1–48
[7] Yan W *et al* 2017 *Nat. Photon.* **11** 514–20
[8] Ledingham K W D *et al* 2000 *Phys. Rev. Lett.* **84** 899–902

[9] Thirolf P G and Habs D 2014 *Eur. Phys. J. Spec. Top.* **223** 1213–9
[10] Gao L, Nilson P M, Igumenshchev I V, Haines M G, Froula D H, Betti R and Meyerhofer D D 2015 *Phys. Rev. Lett.* **114** 215003
[11] http://eli-beams.eu/
[12] Zou J P *et al* 2015 *High Power Laser Sci. Eng.* **3** e2
[13] Hernandez-Gomez C *et al* 2010 *J. Phys.: Conf. Ser.* **244** 032006
[14] Bashinov A V, Gonoskov A A, Kim A V, Mourou G and Sergeev A M 2014 *Eur. Phys. J. Spec. Top.* **223** 1105–12
[15] Di Piazza A, Müller C, Hatsagortsyan K Z and Keitel C H 2012 *Rev. Mod. Phys.* **84** 1177–228
[16] Ridgers C P, Brady C S, Duclous R, Kirk J G, Bennett K, Arber T D, Robinson A P L and Bell A R 2012 *Phys. Rev. Lett.* **108** 165006
[17] Nakamura T, Koga J K, Esirkepov T Z, Kando M, Korn G and Bulanov S V 2012 *Phys. Rev. Lett.* **108** 195001
[18] Brady C S, Ridgers C P, Arber T D, Bell A R and Kirk J G 2012 *Phys. Rev. Lett.* **109** 245006
[19] Bashinov A V and Kim A V 2013 *Phys. Plasmas* **20** 113111
[20] Ji L L, Pukhov A, Nerush E N, Kostyukov I Y, Shen B F and Akli K U 2014 *Phys. Plasmas* **21** 023109
[21] Nerush E N, Kostyukov I Y, Ji L and Pukhov A 2014 *Phys. Plasmas* **21** 013109
[22] Gong Z, Hu R H, Shou Y R, Qiao B, Chen C E, He X T, Bulanov S S, Esirkepov T Z, Bulanov S V and Yan X Q 2017 *Phys. Rev.* E **95** 013210
[23] http://eli-np.ro
[24] Barty C 2011 *CLEO:2011—Laser Applications to Photonic Applications* (https://doi.org/10.1364/CLEO_AT.2011.ATuF2)
[25] http://www.tunl.duke.edu/higs2.php
[26] Bell A R and Kirk J G 2008 *Phys. Rev. Lett.* **101** 200403
[27] Nerush E N, Kostyukov I Y, Fedotov A M, Narozhny N B, Elkina N V and Ruhl H 2011 *Phys. Rev. Lett.* **106** 035001
[28] Jirka M, Klimo O, Bulanov S V, Esirkepov T Z, Gelfer E, Bulanov S S, Weber S and Korn G 2016 *Phys. Rev.* E **93** 023207
[29] Zhu X L, Yu T P, Sheng Z M, Yin Y, Turcu I C E and Pukhov A 2016 *Nat. Commun.* **7** 13686
[30] Gonoskov A, Bashinov A, Bastrakov S, Efimenko E, Ilderton A, Kim A, Marklund M, Meyerov I, Muraviev A and Sergeev A 2017 *Phys. Rev.* X **7** 041003
[31] Vranic M, Grismayer T, Fonseca R A and Silva L O 2017 *Plasma Phys. Control. Fusion* **59** 014040
[32] Chang H X, Qiao B, Huang T W, Xu Zand Zhou C T, Gu Y Q, Yan X Q, Zepf M and He X T 2017 *Sci. Rep.* **7** 45031
[33] Di Piazza A, Hatsagortsyan K Z and Keitel C H 2009 *Phys. Rev. Lett.* **102** 254802
[34] Tamburini M, Pegoraro F, Piazza A D, Keitel C H, Liseykina T V and Macchi A 2011 *Nucl. Instrum. Methods Phys. Res.* A **653** 181–5
[35] Lehmann G and Spatschek K H 2012 *Phys. Rev.* E **85** 056412
[36] Gonoskov A, Bashinov A, Gonoskov I, Harvey C, Ilderton A, Kim A, Marklund M, Mourou G and Sergeev A 2014 *Phys. Rev. Lett.* **113** 014801
[37] Ji L L, Pukhov A, Kostyukov I Y, Shen B F and Akli K 2014 *Phys. Rev. Lett.* **112** 145003
[38] Fedotov A M, Elkina N V, Gelfer E G, Narozhny N B and Ruhl H 2014 *Phys. Rev.* A **90** 053847
[39] Neitz N and Di Piazza A 2013 *Phys. Rev. Lett.* **111** 054802
[40] Bashinov A V, Kim A V and Sergeev A M 2015 *Phys. Rev.* E **92** 043105
[41] Yoffe S R, Kravets Y, Noble A and Jaroszynski D A 2015 *New J. Phys.* **17** 053025
[42] Esirkepov T Z, Bulanov S S, Koga J K, Kando M, Kondo K, Rosanov N N, Korn G and Bulanov S V 2015 *Phys. Lett.* A **379** 2044–54
[43] Bashmakov V F, Nerush E N, Kostyukov I Y, Fedotov A M and Narozhny N B 2014 *Phys. Plasmas* **21** 013105
[44] Bulanov S S, Mur V D, Narozhny N B, Nees J and Popov V S 2010 *Phys. Rev. Lett.* **104** 220404
[45] Gonoskov I, Aiello A, Heugel S and Leuchs G 2012 *Phys. Rev.* A **86** 053836
[46] Landau L D and Lifshitz E M 1975 *The Classical Theory of Fields* (Oxford: Elsevier)
[47] Surmin I A, Bastrakov S I, Efimenko E S, Gonoskov A A, Korzhimanov A V and Meyerov I B 2016 *Comput. Phys. Commun.* **202** 204–10
[48] Fedotov A M, Narozhny N B, Mourou G and Korn G 2010 *Phys. Rev. Lett.* **105** 080402
[49] Narozhny N B, Bulanov S S, Mur V D and Popov V S 2004 *Phys. Lett.* A **330** 1–6
[50] Bulanov S S, Narozhny N B, Mur V D and Popov V S 2006 *J. Exp. Theor. Phys.* **102** 9–23
[51] Gonoskov A, Bastrakov S, Efimenko E, Ilderton A, Marklund M, Meyerov I, Muraviev A, Sergeev A, Surmin I and Wallin E 2015 *Phys. Rev.* E **92** 023305
[52] Nikishov A 1985 *J. Sov. Laser Res.* **6** 619–717
[53] Ritus V 1985 *J. Sov. Laser Res.* **6** 497–617
[54] Bayer V N, Katkov V M and Fadin V S 1973 *Radiation of the Relativistic Electrons* (Moscow: Atomizdat)
[55] Berestetskii V B, Lifshitz E M and Pitaevskii L P 1982 *Quantum Electrodynamics* (New York: Pergamon)